Original paper

Trace-element chemistry of barren and ore-bearing quartz of selected Au, Au–Ag and Sb–Au deposits from the Bohemian Massif

Karel PACÁK[1], Jiří ZACHARIÁŠ[1]*, Ladislav STRNAD[2]

[1] *Institute of Geochemistry, Mineralogy and Mineral Resources, Charles University, Albertov 6, 128 43 Prague 2, Czech Republic; jiri.zacharias@natur.cuni.cz*
[2] *Laboratories of the Geological Institutes, Charles University, Albertov 6, 128 43 Prague 2, Czech Republic*
[*] *Corresponding author*

The trace-element contents in gold-bearing and barren quartz veins from eight Au, Au–Ag and Sb–Au Variscan deposits in the Bohemian Massif have been determined *in situ* in order to evaluate the differences between the various types of gold deposits and discuss trace-element variations in the successive generations of quartz veins. The variability of Ti, Al, Ge, Li and Sb abundances obtained by Laser-Ablation Inductively-Coupled Plasma Mass Spectrometry (LA-ICP-MS) roughly correlates with the origin and the temperature of the mineralizing fluids. The Al content ranges up to 4020 ppm (median value 230 ppm), while the Li content is generally low (< 4 ppm). The elevated Sb content (30–360 ppm Sb) is only related to quartz that immediately preceded deposition of Sb-rich phases. The titanium content of the ore-bearing vein quartz follows bimodal distribution: gold deposits with assumed higher temperature (> 450 °C) formation exhibit higher median values (~10 ppm Ti) than medium-to-low (< 300 °C) temperature deposits (~2 ppm Ti). A statistically significant threshold value (8 ppm Ti) has been recognized as an empirical tool for discriminating between them. In terms of the Ti and Al contents, the studied Bohemian gold deposits fall within and in between fields of orogenic gold and porphyry deposit types.

Keywords: quartz chemistry, titanium, germanium, antimony, gold deposits, LA-ICP-MS
Received: 8 November 2018; accepted: 21 January 2019; handling editor: M. Svojtka
The online version of this article (doi: 10.3190/jgeosci.279) contains supplementary electronic material.

1. Introduction

The formation of minerals can be interpreted as a result of the application of restricting physio-chemical rules to complex natural fluids and melts. Consequently, the chemical composition of the minerals should reflect the environments in which they were formed. This study is focused on the mineral quartz. It is a chemically simple phase, which is stable and occurs in relatively pure form in nature.

The microchemical studies revealed that overall low trace-element contents of quartz reflect the conditions of its formation (Weil 1984; Larsen et al. 2000; Götze and Möckel 2012). Several authors (Landtwing and Pettke 2005; Rusk et al. 2008, 2011; Breiter et al. 2012; Cruz-Uribe et al. 2016; Monnier et al. 2018) have documented the relationships between the trace-element contents in the quartz and its cathodoluminescence characteristics. The Al/Ti and Ge/Ti ratios have been widely used to study the fractionation of granitic and pegmatitic systems (e.g. Müller et al. 2002; Jacamon and Larsen 2009; Breiter and Müller 2009; Breiter et al. 2013, 2014; Garate-Olave et al. 2017). Variations of Ti and Al in individual growth zones can be easily visualized by cathodoluminescence. The Ti content of quartz has a further application as a thermobarometer (Wark and Watson 2006; Thomas et al. 2010, 2015; Huang and Audétat 2012). Given the availability of Laser-Ablation Inductively-Coupled Plasma Mass Spectrometry (LA-ICP-MS) instruments, the number of papers dedicated to quartz chemistry is steadily increasing.

Previous research on quartz from mineral deposits has largely focused on the relationship between cathodoluminescence textures and quartz chemistry (e.g. Rusk et al. 2008) or on the application of mineral thermometry (e.g. Breiter et al. 2012; Monnier et al. 2018). Typically, samples representing contrasting deposit types (e.g., porphyry Cu, orogenic Au, epithermal Au, Mississippi Valley-Type deposits), as well as those with marked differences in luminescence were compared within a single study (e.g. Rusk et al. 2008; Rusk 2012). Recently, detailed LA-ICP-MS works focusing on quartz types/generations from a single deposit have also been published (Müller et al. 2010; Maydagán et al. 2015; Breiter et al. 2017; Wertich et al. 2018).

This contribution focuses on the applicability of quartz microchemistry determined by the LA-ICP-MS technique to crucial questions in ore prospection and exploration, such as: (1) the proper identification of vein types, in case of low to no structural variation between individual veins, (2) quantification of the differences between early-, main-

and late- stage veins and (3) distinguishing between ore-bearing and barren quartz veins. In addition, we have focused on evaluation of the potential of LA-ICP-MS quartz studies in regional exploration for gold deposits.

Most of the samples used in this project are well defined in terms of structural vein types, mineral succession relationships and the pressure–temperature conditions of their formation. All the studied veins were formed within similar to identical geological settings and within a relatively brief time interval (350–330 Ma and ~300 Ma).

2. Geological setting

2.1. Metallogeny of the central part of the Bohemian Massif

Numerous hydrothermal Au, Ag–Pb–Zn and U vein-type ore deposits are located in the central part of the Bohemian Massif, notably along the north-western margin of the Central Bohemian Plutonic Complex (Fig. 1). The formation of most gold deposits (e.g. Morávek et al. 1992; Zachariáš et al. 1997, 2013, 2014) and gold occurrences in this zone broadly overlapped with the intrusive activity of the CBPC (355–335 Ma; Janoušek and Gerdes 2003; Janoušek et al. 2004, 2010); however, some Au–Ag deposits hosted within the Moldanubian Unit are likely younger (~290 Ma; Zachariáš et al. 2009). Numerous Ag–Pb–Zn deposits (e.g. Příbram-Březové Hory, Stará Vožice) most probably postdated the Au-ones, but their absolute age(s) has (have) not yet been determined. The U deposits (e.g. Příbram) are *c.* 280–270 Ma old or younger (Arapov et al. 1984; Anderson 1987; Škácha et al. 2009).

2.2. Central Bohemian Plutonic Complex (CBPC)

The CBPC (3200 km^2) is a stitching pluton that intruded along the boundary between the generally low-grade Teplá–Barrandian and the high-grade Moldanubian units (Fig. 1). It consists of five to seven magmatic suites (Janoušek et al. 1995; Holub et al. 1997) evolving from the oldest calc-alkaline (I-type; ~355 Ma, Janoušek et al. 2004) through potassium-rich calc-alkaline suite (I/S type ~346 to ~336 Ma; Janoušek et al. 2010 and references therein), to the youngest ultrapotassic suite (Tábor Pluton, ~336 Ma; Janoušek and Gerdes 2003). Schulmann et al. (2009) interpreted the CBPC as an Andean-type magmatic arc associated with the subduction of the Saxothuringian ocean beneath the Teplá–Barrandian and Moldanubian units. The resulting crustal thickening (~60 km) led to extensive regional metamorphism (O'Brien and Rötzler 2003) between ~355 and 335 Ma in the Moldanubian Unit.

2.3. Teplá–Barrandian Unit (TBU)

The TBU (Fig. 1) represents part of the Avalonian–Cadomian belt developed along the northern active margin of Gondwana during the late Neoproterozoic (~750 to 540 Ma; e.g. Linnemann et al. 2008). The Neoproterozoic rocks (volcanic, volcanosedimentary and flysh-like sequences; Kříbek et al. 2000) form several juxtaposed, NE–SW trending, allochthonous belts separated by shear zones, interpreted as remnants of the oceanic crust, several accretionary wedges and a single volcanic arc (Hajná et al. 2011). The NNE–SSW trending, 65 km long and 1–6 km wide volcano-sedimentary Jílové Belt is the easternmost part of the TBU. As for the volcanic rocks, the subalkaline Na-rich metabasalts significantly predominate over the metatrachyandesites (Waldhausrová 1984; Fediuk 1992).

2.4 Moldanubian Unit

The Moldanubian Unit (Fig. 1) comprises the metamorphosed pre-Variscan (Precambrian/Early Paleozoic) crust and the Variscan granitoids (e.g. Dallmeyer et al. 1995; Franke 2000). The unit is further subdivided into the Gföhl, Monotonous and Varied units. The former one underwent Variscan HP–HT metamorphism, followed by subsequent rapid exhumation and re-equilibration under mid-crustal conditions (e.g. Franěk et al. 2011a, b). The latter two only recorded mid-crustal LP–HT metamorphism (at *c.* 335 Ma; Friedl 1997; O'Brien 2000). The Gföhl Unit is interpreted as orogenic lower crust (Schulmann et al. 2005, 2008). The main rock types forming the Gföhl Unit are leucocratic granulites and migmatitic orthogneisses accompanied by subordinate mantle peridotite and eclogite, while the Monotonous Unit is dominated by paragneiss and Varied Unit by paragneiss, orthogneiss, marble, quartzite, and amphibolite.

2.5. A brief summary of the studied deposits

Based on ore-related phases/elements, the gold deposits in the study area can be effectively classified into three subgroups (e.g. Bernard 1981; Bernard et al. 1983), as follows.

2.5.1. High-fineness Au deposits ("Au")

Characteristically, the gold at high-fineness Au deposits (herein refered to as "Au" deposits) is accompanied by accessory Bi–Te–S phases; scheelite is common and molybdenite minor; the gold fineness is typically > 900 (e.g., Mokrsko, Jílové, Petráčkova hora, Kasejovice and the Libčice deposits). All the deposits were formed between

348 and 338 Ma (Zachariáš and Stein 2001; Zachariáš et al. 2001, 2013; Ackerman et al. 2017, in print).

2.5.2. High-fineness Sb–Au deposits ("Sb–Au")

In this subgroup, gold fineness > 850; characteristic are mineable stibnite, minor aurostibite, no scheelite, almost no molybdenite, accessory Pb–Sb sulfosalts, extremely rare Bi–Te–S phases (e.g., Krásná Hora and Příčovy deposits). The Sb–Au-bearing veins are spatially associated with lamprophyre dykes and caused their extensive hydrothermal alteration (Němec and Zachariáš 2018). The "Sb–Au" deposits are thus younger than the lamprophyre dykes in the central part of the CBPC. However, a similar lamprophyre dyke located much farther to the W of the Krásná Hora deposit has been dated to 338 ± 0.5 Ma ($^{40}Ar/^{39}Ar$; Žák et al. 1998). The Sb–Au deposits ought to be younger than ~338 Ma and are probably older than ~330 Ma.

2.5.3. Low-fineness Au–Ag deposits ("Au–Ag")

At low-fineness (< 700) deposits occur arsenopyrite and As-pyrite; completely lacking are W–Mo–Bi–Te–S–Sb phases (e.g., the Roudný deposit; Zachariáš et al. 2009). These deposits are related to the major-to-minor brittle-fault zones within the LP–HT parts of the Moldanubian Unit (i.e., they are located to the E, SE, or S of the CBPC). Unfortunately, the low-fineness Au–Ag deposits have not yet been dated. An age of ~290 Ma is anticipated, based on their relationship to the Carboniferous sedimentary infill of the Blanice Furrow (Pták 1962).

3. Samples and methods

3.1. Classification of the quartz veins

The samples used in this study were largely collected during our previous studies (Tab. 1). Classification of the quartz veins (Q0–Q5) is based on the field observation of the crosscutting relationships between successive generations. In addition, when appropriate, samples of the magmatic (Qgrnd – granodiorite) or the pegmatite (Qpeg) quartz of an intrusion hosting a deposit were included

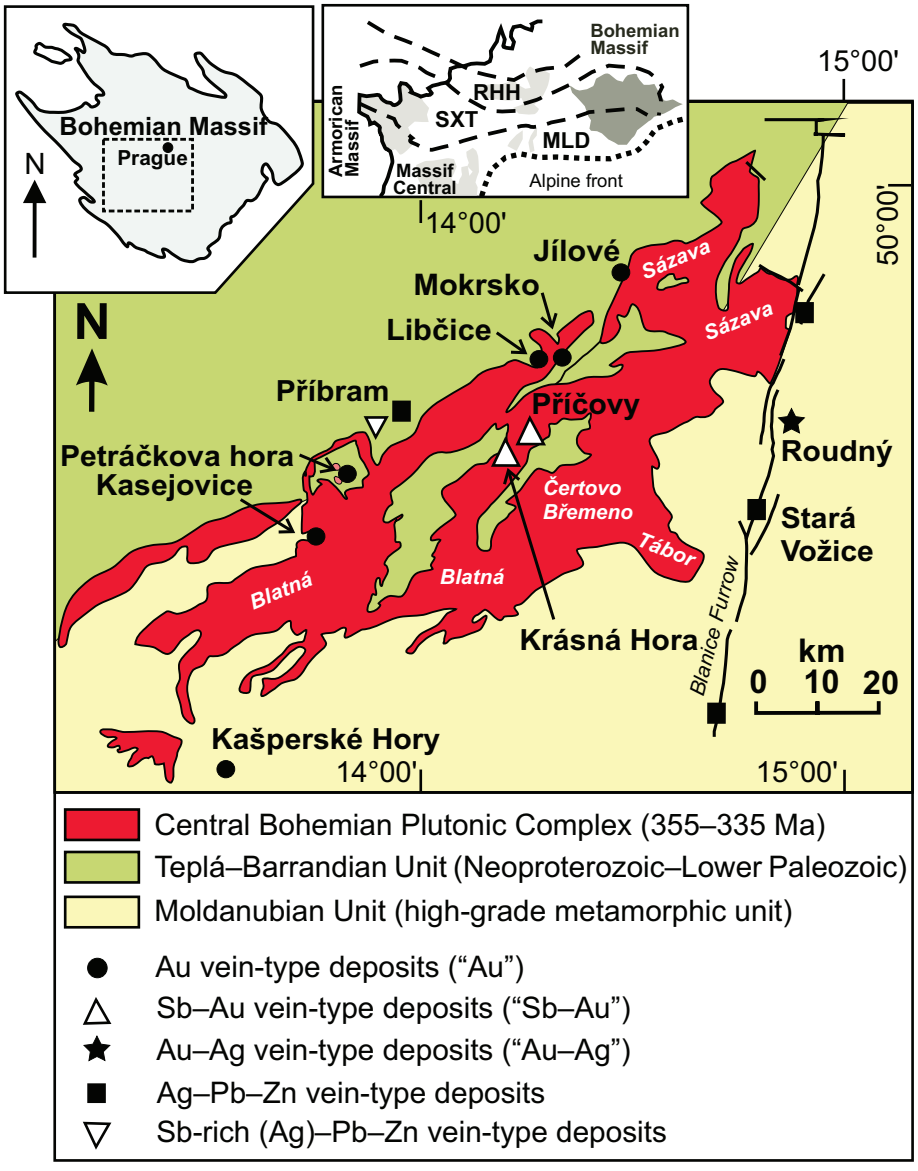

Fig. 1 A schematic geological map of the Central Bohemian Plutonic Complex (CBPC) and its surroundings. Small insets show position of the studied area in the Bohemian Massif and localization of the Bohemian Massif with respect to the distribution of Variscan zones in Europe: Saxothuringian (SXT), Rhenohercynian (RHH) and Moldanubian (MLD). The individual groups of Variscan vein-type hydrothermal ore deposits are differentiated by symbols. The rough positions of the individual major plutons within the CBPC mentioned in the text are indicated by white text (Sázava, Blatná, Čertovo břemeno and Tábor).

Tab. 1 A simplified summary of the geology, ore resources, quartz vein types and vein formation conditions for the studied deposits

Deposit	Subtype (genetic type)	Gold resources, host rock	Vein types General characterization and abundance	References Formation conditions
Petráčkova hora	*high-fineness Au* (IRG)	~33 t @ 1.1 g/t Au or ~7 t @ 2.0 g/t Au granodiorite	Q1 – sparse, early ore veins with K-feldspar alteration rim Q2 – abundant, main ore veins, no alteration, scheelite-bearing, up to 50 g/t Au Q3 – minor, main ore veins, no alteration, abundant scheelite Q4 – abundant, later phase of ore veining, no alteration, sparse scheelite, usually < 10 g/t Au Q5 – minor, late veins (traces of Au only), related to marked change in regional stress orientation (minor) Qx – sparse, barren quartz veins, distal (*c.* 1 km E of the deposit), hosted by low-grade Paleozoic meta-sandstones, probably post-ore	Zachariáš et al. (2001) Q1: 570–530 °C Q2–Q3: 490–450 °C Q5: ~300 °C Qx: ~200 °C
Mokrsko-West	*high-fineness Au (IRG/ORG)*	~90 t @ 1.8 g/t Au granodiorite	Q0 – minor, pre-ore barren subhorizontal veins Q1 – early ore veins (subvertical, more than 20 cm thick) Q12 – abundant, main ore veins, sheeted complex of vertical 10–3 cm thick veins (they may represent Q1 or Q2 types, or a transition between them) Q2 – very abundant, main ore veins, sheeted complex of densely spaced vertical veinlets < 5 mm thick Q3 – sparse, moderately dipping, post-Q2 veins	Morávek et al. (1989); Boiron et al. (2001); Zachariáš et al. (2014); Zachariáš (2016) Q1, Q12, Q2, Q3: > 450 °C and 2.5–3.6 kbar
Libčice	*high-f. Au IRG/ORG*	~0.1 t Au @ 7–18 g/t Au metasediments, metavolcanites	Q1 – single quartz vein (up to 2 m thick) that underwent thermal static recrystallization due to thermal metamorphism by the CBPC	Hrstka et al. (2011) Q1: > 350 °C
Kasejovice	*high-f. Au (ORG)*	~700 kg Au @ ~10 g/t Au HT–LP gneiss	Q1 – main quartz, represents bulk of the gangue, associated with wolframite and arsenopyrite Q2 – late quartz, volumetrically minor, associated with Au–Bi–Te phases Q2 – late quartz, volumetrically minor, associated with Pb–Sb–S phases	Zachariáš et al. (1997); Zachariáš and Pudilová (2002) Q1: 350 °C Q2: 250 °C Q3: 200 °C
Jílové	*high-fineness Au (ORG)*	~10 t @ 6 g/t Au metavolcanites (& granodiorite porphyry)	Q0 – subhorizontal veins at periphery of the district, probably pre-ore Q1–Q2 – main veins, gold-bearing Q3 – late quartz filling fractures in Q1–Q2, it is associated with native arsenic and base-metal sulphides	Morávek (1971), Zachariáš et al. (2013) Q2: 320–280 °C Q3: 200–150 °C
Krásná Hora	*high-fin. Sb–Au (ORG)*	~1.5 t @ 3–5 g/t Au lamprophyre dykes within granodiorite	Q1 – early veins with sparse arsenopyrite (most of them are Au-barren) Q2 – main ore veins associated with deposition of stibnite Q3 – late ore quartz (Q3), fills in fractures in Q2 or Q1, predates/accompany gold	Zachariáš and Němec (2017); Němec and Zachariáš (2018) Q1: 300–400 °C, 1–2.5 kbar Q2: 280–330 °C, 0.5–1.3 kbar Q3: 200–240 °C, 0.4–1.0 kbar
Příčovy	*high-fin. Sb–Au (ORG)*	~0.5 t @ 9.4 g/t Au lamprophyre and granod. porphyry dykes within granodiorite	Q1 – not present at the deposit Q2 – quartz similar to that of the Krásná Hora deposit, occurring as early fine-grained (Q2a) and late coarse-grained (Q2b) subtypes, associated with stibnite and zinkenite	Němec and Zachariáš (2018) Q2: about 300 °C and 0.5–1.3 kbar
Roudný	*low-fineness Au–Ag (ORG)*	~6 t @ 10 g/t Au altered gneiss	Q1 – sparse early quartz veins (Q1) with tourmaline (of unclear relation to ore-mineralization, may represent late-metamorphic veins) Q2 – ore-related veins, abundant As-bearing pyrite and arsenopyrite (both contain invisible gold) Q3 – late quartz (Q3) fill (early phase of formation of Q3 is associated with deposition of macroscopic gold)	Zachariáš et al. (2004, 2009), Zachariáš and Hübst (2012) Q1: 350–420 °C, 1.6–1.9 kbar Q2: 330–380 °C, 0.3–0.6 kbar Q3: 170–230 °C, 0.3–0.5 kbar

IRG – intrusion-related gold deposit, ORG – orogenic gold deposit, Q – quartz vein type

Tab. 2 The concentrations of the selected elements (median values; ppm) for the studied gold deposits and quartz/vein types

Deposit	Quartz	n	Li	Na	Al	K	Ti	Mn	Ga	Ge	As	Rb	Sr	Sb	Cs	Ba	Pb
Mean det. limits			0.3	125	50	15	1.5	0.4	0.1	0.1	0.1	0.1	0.2	0.5	0.1	0.4	0.1
Mokrsko	Qgrnd	17	0.9	–	347	129	47	5.3	0.3	0.6	0.8	0.7	2.5	0.8	0.2	3.3	0.2
Mokrsko	Qpeg	17	4.0	–	261	47	11	15.7	0.3	3.0	–	0.6	0.7	0.7	0.2	0.7	0.2
Mokrsko	Q0	15	6.3	297	177	29	21	0.6	–	0.7	0.5	0.2	0.6	0.9	–	1.1	0.3
Mokrsko	Q1	116	1.7	–	223	29	9	1.3	0.3	1.9	1.3	0.4	0.9	0.8	0.5	1.5	0.6
Mokrsko	Q12	171	2.8	–	194	35	10	1.1	0.4	1.5	1.0	0.3	0.9	1.7	0.2	1.0	0.3
Mokrsko	Q2	157	3.8	181	205	35	8	3.3	0.3	1.8	1.3	0.3	1.5	1.1	0.8	1.7	0.4
Mokrsko	Q3	11	1.2	–	78	25	6	1.1	0.4	1.5	0.9	0.2	1.9	0.6	0.3	0.6	0.2
Petráčkova hora	Qgrnd	6	0.8	667	317	61	75	4.6	0.5	0.5	1.7	1.2	1.5	0.8	0.3	5.5	2.0
Petráčkova hora	Qpeg	8	–	316	464	47	77	6.1	0.2	1.2	1.2	0.8	1.2	0.6	0.3	0.8	1.6
Petráčkova hora	Q1	7	0.6	1052	398	42	15	2.0	1.1	4.3	2.5	1.0	1.5	1.3	0.3	3.7	0.6
Petráčkova hora	Q2	11	0.5	467	206	34	20	4.0	0.2	2.5	3.7	0.8	1.0	0.6	0.3	0.7	0.4
Petráčkova hora	Q2–Q3	11	0.7	539	379	76	28	5.5	0.3	1.7	1.5	0.9	3.1	0.7	0.3	1.1	0.9
Petráčkova hora	Q4	21	0.8	433	251	42	16	3.0	0.3	2.2	1.9	0.4	3.0	1.0	0.3	0.5	1.0
Petráčkova hora	Q5	9	1.2	1957	467	228	31	26.7	0.5	1.9	3.2	2.5	3.6	1.8	3.0	1.2	14.8
Petráčkova hora	Qx	6	0.9	638	819	91	2	1.0	0.3	1.5	1.7	0.7	1.0	1.1	0.2	1.7	0.8
Jílové	Q0	20	0.5	350	159	16	–	0.7	0.2	0.4	1.0	0.2	0.7	0.9	0.3	2.7	0.5
Jílové	Q1a	45	0.6	520	107	20	2	0.5	0.3	1.0	1.7	0.3	0.7	1.9	0.3	0.7	0.3
Jílové	Q1b	14	0.6	413	222	31	2	–	0.2	1.1	1.5	0.2	0.7	15.3	0.3	0.9	0.2
Jílové	Q2	7	0.4	290	77	28	5	0.5	–	0.4	1.4	–	0.4	0.7	–	–	0.2
Jílové	Q3	6	0.5	639	59	25	2	0.5	0.2	0.9	1.7	0.2	0.5	0.9	0.2	0.5	0.3
Kasejovice	Q1	50	0.7	810	168	371	6	0.7	0.4	1.3	0.6	0.9	0.5	1.5	0.4	1.4	0.3
Kasejovice	Q2	21	1.3	518	161	35	–	2.9	0.4	0.7	0.7	0.3	1.0	43.5	0.5	2.0	0.3
Kasejovice	Q3	12	1.0	526	2632	391	2	0.6	0.3	0.8	0.5	2.5	2.7	3.6	0.5	19.2	0.3
Libčice	Q1r	25	4.3	316	122	18	4	1.0	0.3	0.6	0.5	0.2	0.5	1.0	0.3	1.2	0.3
Roudný	Q1	13	0.7	230	301	24	31	6.9	0.3	1.5	0.6	0.2	0.6	–	0.2	4.1	0.7
Roudný	Q12	10	2.7	374	240	26	9	6.1	0.2	0.9	0.4	0.3	0.4	–	0.2	2.2	1.2
Roudný	Q2	20	1.0	587	3157	164	2	4.4	0.5	1.7	0.9	1.6	9.6	7.4	1.5	28.1	0.3
Roudný	Q3	7	1.0	889	2789	163	3	3.6	0.7	1.0	0.8	1.5	15.5	3.3	1.3	46.3	0.4
Krásná Hora	Q1	27	1.5	329	278	21	18	0.8	0.2	0.7	0.9	0.3	1.9	3.3	0.3	2.4	1.5
Krásná Hora	Q2	77	0.8	238	518	38	3	0.6	0.3	3.1	1.6	0.3	0.5	115.2	0.2	1.3	0.4
Příčovy	Q2P	5	6.7	–	370	25	25	–	–	–	1.6	0.7	1.0	1.0	–	2.7	1.0

For the complete data set, including the detection limits, see the Electronic Supplement

in the study. The labels (Q0–Q5) used for the individual vein types (quartz generations) represent the succession of the studied veins and, as such, are unique for each of the investigated deposits.

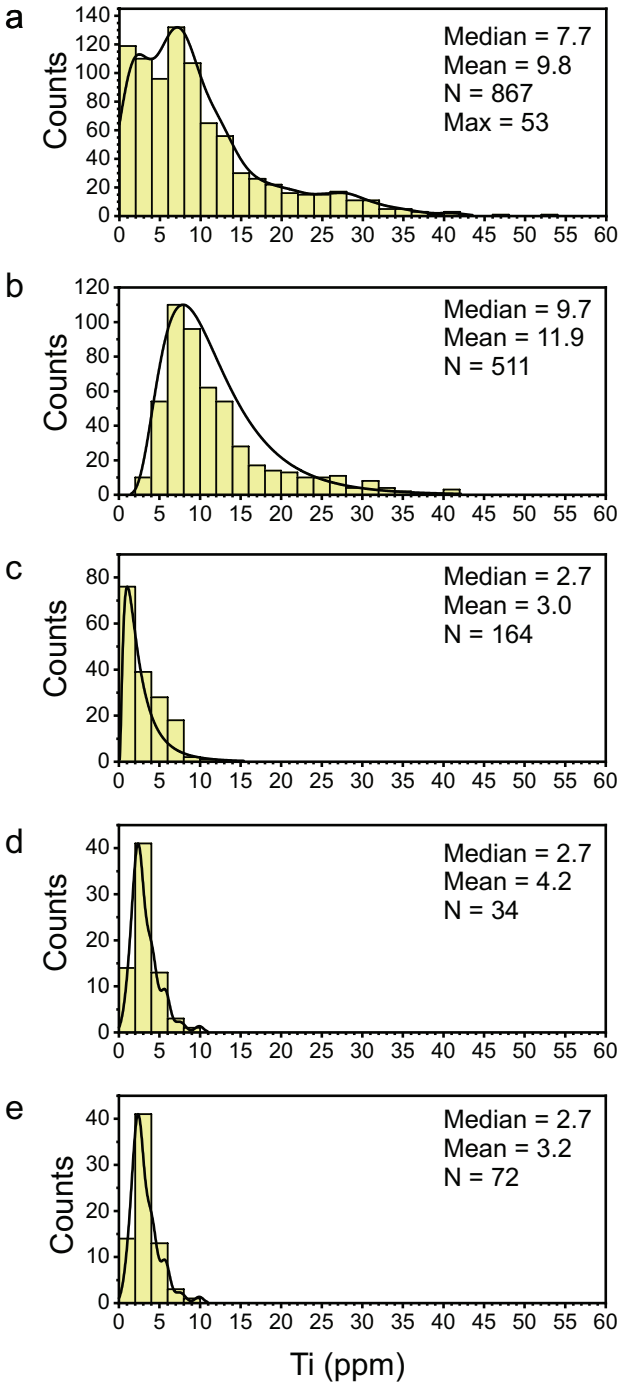

Fig. 2 Distribution of Ti in the hydrothermal quartz veins from the studied deposits; **a –** all the veins altogether, both ore-bearing and barren; **b –** ore-bearing veins at the "high-temperature Au" Mokrsko and Petráčkova hora deposits; **c –** ore-bearing veins at the "medium-to-low temperature Au" Jílové, Kasejovice, and Libčice deposits; **d –** ore-bearing veins at the "medium-to-low temperature Au–Ag" Roudný deposit; **e –** ore-bearing veins at the "medium-to-low temperature Sb–Au" Krásná Hora deposit.

To retain clarity in the text/charts across the deposits, the vein quartz generations were grouped into various evolutionary stages, denoted by the previous prefixes:

- *pre-* barren quartz veins predating the formation of ore-bearing veins;
- *early-* early/first generation(s) of quartz veins, rare to minor in abundance, marginally associated with the ore formation;
- *main-* the main stage of the formation of the quartz veins (i.e., the stage when the bulk of the quartz mass precipitated). This stage may be associated with the ore formation; however, the bulk of the Au (Sb) ore typically postdates the main stage;
- *ore-* quartz directly associated with the precipitation of the ore;
- *late-* quartz that has been proven to postdate the formation of the main veins. Minor in abundance, sub-economic in grade;
- *post-* the barren quartz that has been demonstrated to postdate the formation of the ore-related veins.

3.2. Optical cathodoluminescence (CL)

Prior to the ablation, all the samples were inspected by the optical CL. We observed thin zones (< 10 μm) of contrasting luminescence in otherwise homogeneous samples. The observed zones are related to quartz recrystallization along the grain boundaries, to microfractures, or to rare growth zones (e.g. Wertich et al. 2018). These zones represent insignificant fraction of the ablated volume (see below). Wertich et al. (2018) focused on similar types of samples/deposits and also concluded that it is nearly impossible to analyze zones with different CL separately.

3.3. LA-ICP-MS

Samples in the form of 67 thick polished wafers (200–300 μm) were used for the LA-ICP-MS analyses at the Institute of Geochemistry, Mineralogy and Natural Resources of the Faculty of Science, Charles University, using the New Wave laser ablation system (Nd:YAG 213 nm) coupled with the Thermo Scientific iCAP Q mass spectrometer. External calibration of the laser-ablation analyses was performed using the Standard Reference Materials NIST 612 and 610 (National Institute of Standards and Technology, USA) with an internal standardization using ^{29}Si by normalizing to 99.95 wt. % SiO_2. The concentration values for the NISTs of all the measured elements were taken from the GeoReM database (Jochum et al. 2005). The isotopes employed were selected with

respect to their most abundant species, free from an isobaric overlap and minimum interferences. The data were acquired in the time-resolved and peak jumping and the pulse counting mode with one point measured per mass peak (dwell time 12 ms). The ablated material was delivered to the plasma in a continuous stream of helium (1.74 l/min). The formation of oxides (MO^+/M^+) was monitored using U in NIST 612 directly from the ablation and the measured ratios ($^{254}UO^+/^{238}U^+$) varied below a value of 0.009. During the ablation, the sample was manipulated beneath the stationary laser beam to produce a linear pit of *c.* 1000 μm and to minimize the chemical fractionation (e.g. Campbell and Humayun 1999) and fired at a repetitive rate of 10 Hz, using a low laser energy of 0.3 mJ/pulse with a crater diameter of 80 μm. The total acquisition time was 200 s (50 s gas background with 150 s ablation). The data reduction included the correction for the gas blank, the internal standard and a calibration check, and the data were processed off line in an MS Excel spreadsheet-based program (Zachariáš and Wilkinson 2007). Similar analytical protocol and correction strategy have been used by Strnad et al. (2005) and Janoušek et al. (2014).

The measurements on each sample consisted of 6 individual ablation lines, ~1000 μm in length, ~80 μm in width and ~60 μm in depth. The ablation intervals corresponding to "pure quartz" were hand-picked for each ablation line. This has resulted in more than one data set for each line. In total, 942 intervals corresponding to "pure quartz" have been identified. The following isotopes were measured: ^{7}Li, ^{23}Na, ^{25}Mg, ^{27}Al, ^{29}Si, ^{30}Si, ^{31}P, ^{34}S, ^{39}K, ^{43}Ca, ^{44}Ca, ^{49}Ti, ^{51}V, ^{55}Mn, ^{56}Fe, ^{57}Fe, ^{65}Cu, ^{66}Zn, ^{69}Ga, ^{71}Ga, ^{74}Ge, ^{75}As, ^{85}Rb, ^{88}Sr, ^{107}Ag, ^{109}Ag, ^{120}Sn, ^{121}Sb, ^{123}Sb, ^{125}Te, ^{128}Te, ^{133}Cs, ^{138}Ba, ^{182}W, ^{183}W, ^{197}Au, ^{208}Pb, ^{209}Bi, ^{232}Th, and ^{238}U. The statistical analysis of the data was performed in Origin® and Excel® (descriptive statistics) and in IBM® SPSS® (nonparametric tests).

The external replication of this method was monitored using a USGS BCR-2G glass reference material (e.g. Norman et al. 1998; Tiepolo et al. 2003). We firmly believe that the results for Ti in quartz veins at the Mokrsko–West deposit are in agreement with a recently published independent study (Wertich et al. 2018). The following statistical parameters are included for comparison: our dataset (N = 452, min = 2, max = 35, mean = 10.7, median = 9.0) vs. data digitalized from fig. 6 of Wertich et al. (2018) (N = 48, min = 1.2, max = 62, mean = 9.1, median = 6.2).

4. Results

Eight gold deposits in total, representing the three subgroups, were selected for this study (Tab. 1, Fig. 1). The deposits span a wide range of formation conditions (from > 500 to less than 200 °C, and from 6 down to 0.5 kbar) and a range from world-class (~100 t of Au in resources) to non-economic (< 1 t Au). All the deposits are located in a small area of approximately 70 × 50 km. For a summary of the vein generations distinguished at each deposit, see Tab. 1 and the references mentioned in this table.

Table 2 presents the median values of the selected elements within quartz veins at various kinds of gold deposits in the central part of the Bohemian Massif. The complete descriptive statistics, as well as a full set of analytical data can be found as an electronic supplement material (ESM). Most of the analyzed elements display log-normal distributions (Fig. 2). Therefore, the median instead of the mean values are presented throughout the text and in Tab. 2. The abundance of the selected elements (Ti, Al and Ge) is also presented as X–Y plots, given separately for the higher-temperature (Fig. 3) and medium- to low- temperature (Fig. 4) deposits.

4.1. Titanium

The measured Ti content of the ore-related quartz vein exhibits bimodal distribution (Fig. 2a) when all the data are treated collectively. The higher-temperature "Au" deposits show elevated Ti contents (Fig. 2b; median 9.7 ppm; 9.1 and 17.2 ppm for Mokrsko and Petráčkova hora, respectively) compared to the other "Au" (median 2.3 ppm; Fig. 2c) and "Sb–Au" deposits (median 3.7 ppm; Fig. 2e).

The early and probably barren Q1 veins with ambiguous genetic and temporal relationships to the ore-related veins were identified at the "Sb–Au" Krásná Hora and "Au–Ag" Roudný deposits. These veins contain about 18 and 31 ppm Ti, respectively (Tab. 2), which is significantly more than was measured in the ore-related veins (2–3 ppm Ti in Q2–Q3; Tab. 2) in these deposits.

Quartz of magmatic origin yielded the highest observed Ti contents (up to 89 ppm). The Ti median values the groundmass quartz range from 75 ppm in the granodiorite of the Petráčkova hora "Au" deposit (Fig. 3a) to 47 ppm in the Sázava granodiorite–tonalite of the Mokrsko "Au" deposit (Fig. 3b). The pegmatitic quartz exhibited median values similar to that of the hosting granodiorite (77 ppm Ti for the thin aplo-pegmatitic dyke at Petráčkova hora), as well as much lower ones (11 ppm at Mokrsko; a small pegmatitic body in the exocontact of the Sázava tonalite).

4.2. Aluminum, gallium and germanium

The element contents in most of the analyzed samples vary from below the detection limits to up to 4021 ppm Al, up to 1.9 ppm Ga and up to 12.4 ppm Ge (Figs 3–4).

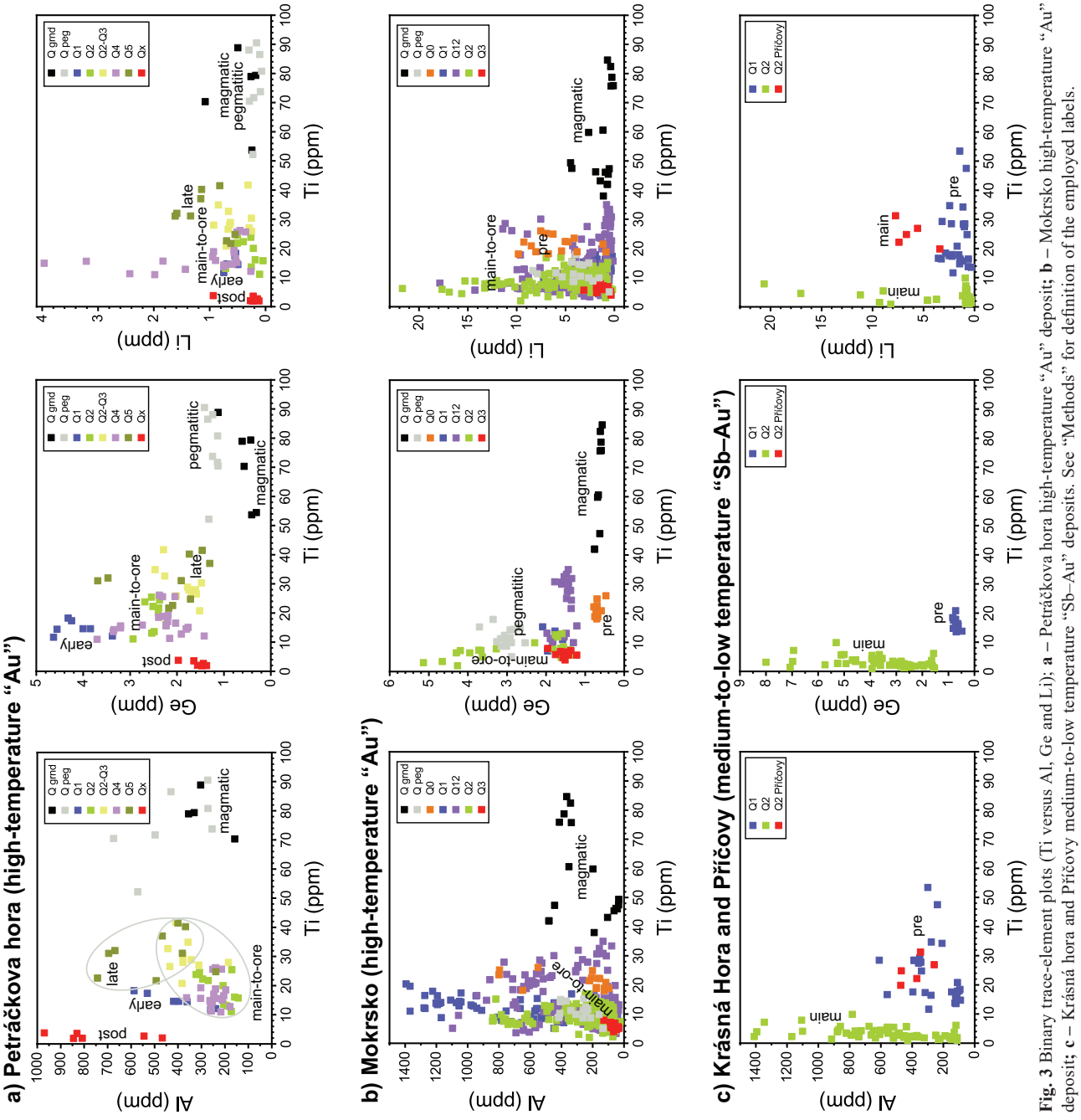

Fig. 3 Binary trace-element plots (Ti versus Al, Ge and Li); **a** – Petráčkova hora high-temperature "Au" deposit; **b** – Mokrsko high-temperature "Au" deposit; **c** – Krásná hora and Příčovy medium-to-low temperature "Sb–Au" deposits. See "Methods" for definition of the employed labels.

No obvious correlation between Al and Ga, or Ga and Ge has been observed in the analyzed samples.

4.3. Lithium, rubidium, cesium, strontium, barium, potassium and sodium

Lithium, rubidium, cesium, strontium and barium abundances exhibit lognormal distributions, with following median ppm values: 1.6 (Li), 0.4 (Rb), 0.3 (Cs), 0.9 (Sr) and 1.4 (Ba). The highest observed ppm values are 22 (Li), 10 (Rb), 6 (Cs), 19 (Sr) and 67 (Ba). The Ba content above 10 ppm corresponds to about 4% of the values obtained in our analyses. The absence of Ba and S covariation suggests that there is no contamination by barite microinclusions. Because of the high detection limits for Na and K, these elements are not discussed in detail.

4.4. Lead and antimony

The lead content varies from 0.1 to 4 ppm in most samples. Slightly higher values are limited to the late

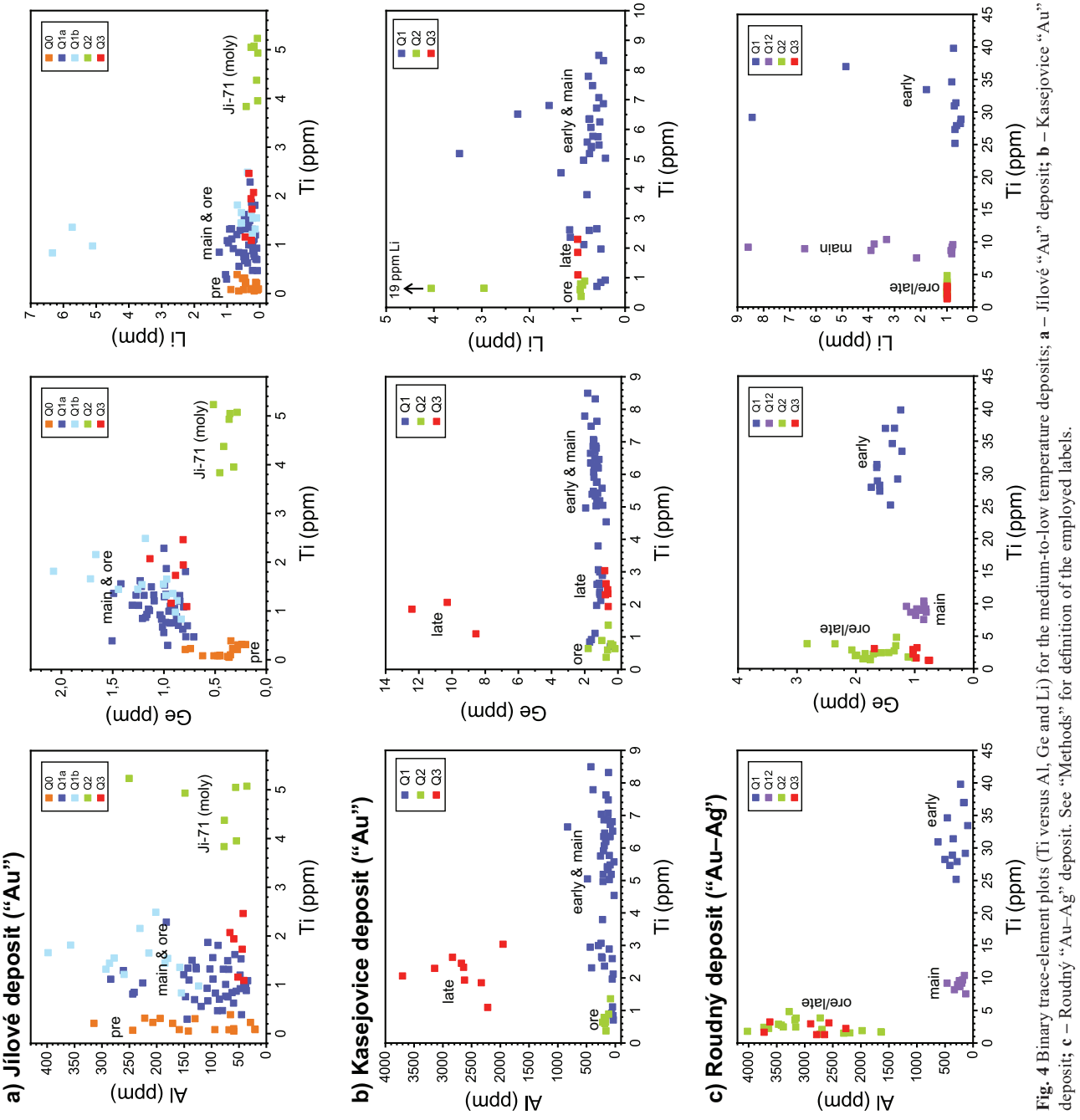

Fig. 4 Binary trace-element plots (Ti versus Al, Ge and Li) for the medium-to-low temperature deposits; **a** – Jílové "Au" deposit; **b** – Kasejovice "Au" deposit; **c** – Roudný "Au–Ag" deposit. See "Methods" for definition of the employed labels.

Q5 quartz from the Petráčkova hora "Au" deposit (3–21 ppm Pb; median 15 ppm). Antimony is a very common trace element found in most analyzed quartz samples, with median values typically below 3 ppm. Higher median values were observed for deposits where Sb-bearing phases are common. This includes the Roudný (7 ppm in Q2; Sb-rich arsenopyrite), Jílové (15 ppm in Q1b; unconfirmed phase), Kasejovice (44 ppm in Q2; Sb-bismuthinite, jamesonite, berthierite), and Krásná Hora (115 ppm in Q2; stibnite) deposits.

5. Discussion

5.1. Differences in the Ti contents – the temperature effect

The concentration of Ti in the ore-related hydrothermal quartz from the analyzed gold deposits exhibits a bimodal distribution (Fig. 2a). The median value of 9.7 ppm Ti (up to ~50 ppm) was observed in the "Au" deposits with a high-temperature origin (> 450 °C; Mokrsko and Petráčkova hora; Figs 2b and 3a–b). Quartz from the

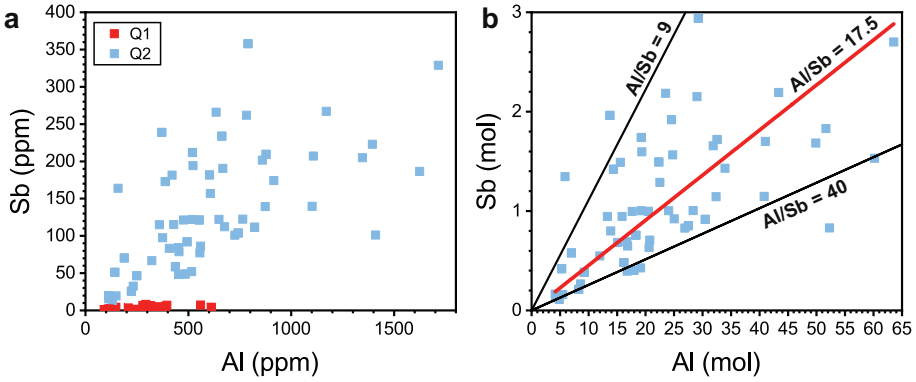

Fig. 5 Positive correlation between the contents of Al and Sb for samples from the Krásná Hora "Sb–Au" deposit: **a** – weight-unit (ppm) plot for the Q1 and Q2 veins; **b** – molar plot for Q2 veins alone. Molar ratios (Al/Sb) are indicated by labelled lines. The red line represents a linear fit of all Q2 data with intercept fixed at origin.

medium- (< 350 °C) to low- (~200 °C) temperature "Au" deposits typically exhibits a median value of 2.7 ppm Ti (Fig. 2c–d and Fig. 4a–b).

Non-parametric statistical tests have confirmed that the Ti median values and the data distributions for the high-temperature (Fig. 2b) and medium- to low-temperature (Fig. 2c) deposits are statistically different at a significance level of 0.05 (Mann-Whitney U test: U = 85451, n1 = 166, n2 = 521, P < 0.05; Median test: grand median = 8.048, n = 687, test value = 202.740, Chi-square = 200.210). A very low p-value ($p < 2.2e^{-16}$; Wilcoxon test) refutes the null hypothesis that all of the Ti data represent a single population. To conclude, the Ti content in the hydrothermal quartz may help to differentiate the higher-temperature veins from the majority of the low-to-medium temperature veins, even if the exact application of Ti thermometry is still questionable/difficult (especially because of the uncertainty in the activity of titanium during the quartz formation).

5.2. Distinguishing the quartz generations based on differences in the Ti contents

For some deposits, unambiguous discrimination between early (and often barren) and late (and ore-bearing) generations of quartz veins was possible solely on the basis of the Ti content of the quartz. The early veins contain significantly more Ti (~20 to ~30 ppm) than the late ones (< 10 ppm Ti). For example, two main types of quartz veins have been identified at the "Sb–Au" Krásná Hora deposit (Němec and Zachariáš 2018): barren pre-ore veins (Q1; barren with respect to Au and Sb), and the main- to ore-stage veins (Q2). The Q2 quartz contains less than 10 ppm Ti (median 3 ppm), while the concentrations in the Q1 quartz range from ~11 to over 50 ppm Ti (median 18 ppm). The Q1 and Q2 quartz also differ in the nature of the trapped fluids (H_2O–CO_2 vs H_2O, respectively) and the temperature of formation (~400 vs. ~300 °C; see Němec and Zachariáš 2018).

A similar pattern can be observed at the "Au–Ag" Roudný deposit. Early and barren quartz veins (Q1, Zachariáš et al. 2009) contain 31 ppm Ti (median value), while the ore-bearing ones exhibit much lower median values: 9 ppm for Q12 quartz associated with impregnations of Au-bearing arsenopyrite (Au-1, "invisible gold"); and 2–3 ppm for Q2 and Q3 associated with macroscopic gold (Au-2). The Q1 quartz was precipitated from aqueous–carbonic fluids, while Q2–Q3 was formed from aqueous-only fluids at a lower temperature than Q1.

5.3. Antimony content in the quartz

Generally, the content of Sb in samples is less than 4 ppm, with the exception of the Q1b quartz from Jílové (9–36 ppm Sb) and the Q2 quartz from Roudný (2–19 ppm Sb). In addition, two of the studied deposits contain more than 30 ppm Sb (up to 190 ppm in Q2 and Q3 from the "Au" Kasejovice deposit; and up to 358 ppm in Q2 from the "Sb–Au" Krásná Hora deposit). Positive correlation between Al and Sb contents can be observed at Krásná Hora (Q2; Fig. 5). The above-mentioned Q2 quartz is very transparent and free of ore (stibnite) microinclusions. These, if present, are related exclusively to late fractures or to the latest Q2 growth zone (Němec and Zachariáš 2018). The absence of sulfur in our measurements excludes possible contamination by stibnite. The molar ratio for Al/Sb varies from 40 to 9 (Fig. 5b). The linear fit of data through the origin approaches a ratio of 20.

The Sb contents of magmatic and hydrothermal quartz have been rarely reported. Monnier et al. (2018) gave maximum values of 4.5 ppm for magmatic quartz, 161 ppm for stibnite-bearing hydrothermal quartz and from several ppm up to *c.* 70 ppm for various hydrothermal quartz veins with no association with stibnite. The data provided in Monnier et al. (2018) suggest no correlation between Al and Sb.

5.4. Evidence for switching between various fluid-source reservoirs

The trace-element composition of the hydrothermal quartz can be interpreted as being a result of three main

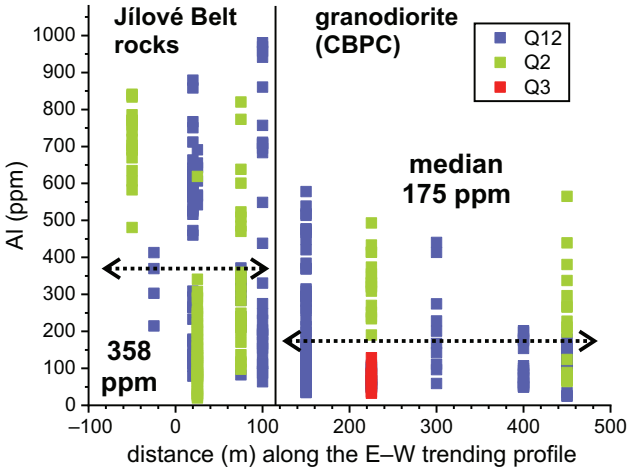

Fig. 6 Variations in the Al content of the Q12, Q2 and Q3 veins along the E–W trending profile across the Mokrsko–West deposit. The thick dotted lines show the mean Al values within the different lithological blocks (meta-volcano-sedimentary rocks vs. granodiorite).

variables: (1) the original fluid phase composition that reflects, in part, the fluid–rock (and/or fluid–magma) interactions in the fluid source region, (2) the actual physicochemical conditions during the quartz precipitation and (3) various kinetic effects (e.g. Monecke et al. 2002; Rusk et al. 2008, 2011). The quartz related to substantially different fluids may exhibit distinct elemental abundances and/or ratios. Below we discuss three case examples of such a situation:

5.4.1. Petráčkova hora (a high-temperature "Au" deposit)

This deposit exhibits the most obvious links between the magmatic history of the host intrusion and the P–T–X and genetic evolution of the hydrothermal quartz veins (both barren and ore-bearing). A negative correlation between the Ti and Ge abundances in the quartz of magmatic (Qgrnd, Qpeg) and early hydrothermal (Q1) origin can be observed if both datasets are considered together. The magmatic quartz exhibits the highest Ti and the lowest Ge contents, while the opposite is true for the hydrothermal (Q1) quartz. This behavior resembles the fractionation trend common in silica-rich melts (i.e., from granite to evolved pegmatite; e.g. Breiter et al. 2014). Therefore, this points to the formation of Q1 veins from a hydrothermal fluid (with a significant contribution of the magmatic component) directly derived from the magma of the host granodiorite (see also Zachariáš et al. 2001).

Compared to the early veins (Q1), the ore-bearing veins (Q2, Q2–Q3, Q4) exhibit a decrease in the Ge content (down to half of the mean value in Q1) and an increase in Ti (up to ~41 ppm; Fig. 3a). Considering their formation from a fluid dominated by a magmatic component (Zachariáš et al. 2001), we interpret the simultaneous decrease in Ge and increase in Ti (both related to Q1) as evidence of a new fluid batch(es). Such batch(es) should be genetically associated with a similar magmatic source. However, it should be seated deeper than those linked with the host intrusion (and related to Q1 veins). This is possible if we consider the location of the Petráčkova hora deposit/intrusion at the periphery of the voluminous Blatná granodiorite pluton (both bodies are similar in age and geochemistry) of the CBPC.

The youngest Q5 veins formed after a distinct change in the orientation and magnitude of the regional stress (Zachariáš et al. 2001). This suggests a time gap between the formation of the Q1–Q4 and Q5 veins. The distinct trace-element signature of the Q5 quartz is compatible with the proposition of opening a new fluid migration path, tapping a new fluid source.

5.4.2. Mokrsko (a high-temperature "Au" deposit)

Under regional stress, the barren pre-ore (Q0) veins at the Mokrsko "Au" deposit developed orientation distinct from that during the gold deposition (Q1, Q2, Q3; Zachariáš 2016). The Q0 quartz differs by higher Ti (~20 ppm), Li (~6 ppm) and lower Ge (~0.7 ppm) contents (Fig. 3b) from the Au-bearing quartz (Q1–Q3; 6–11 ppm Ti, 1–4 ppm Li, 1.5–1.9 ppm Ge). In contrast, it is impossible to differentiate between the individual ore-bearing veins (Q1, Q12, Q2), based on the quartz trace-element contents alone. This suggests similar, or the same, fluid source for the ore-bearing veins and a substantially different fluid source for the Q0 veins. Furthermore, the content of Al in Q1 through Q3 seems to be affected by the host-rock lithology (Fig. 6; for the detailed geology, see Zachariáš 2016).

5.4.3. Jílové (a medium-temperature "Au" deposit)

The Jílové deposit is hosted by similar lithological units (the Jílové Belt of the TBU and granodiorite porphyry dykes of the CBPC) as the Mokrsko deposit. However, the Jílové deposit is structurally different, of a lower temperature nature and younger (~339 Ma; Zachariáš et al. 2013). The pre-ore barren (Q0) veins at Jílové, although similar in orientation to the pre-ore barren (Q0) veins at Mokrsko, exhibit Ti content below the detection limit (1.5 ppm). The observed abundance of Ti is almost 20× higher (~20 ppm) in the Q0 veins at the Mokrsko deposit. Such a divergence implies distinct formation temperatures and the age of the Q0 veins at the two deposits.

The only sample with a strikingly different composition in the Jílové dataset (Q2–Q3) is Ji-71 (initially classified as a Q2 vein). This sample, about a 1 cm thick

vein with coarse-grained quartz intergrown with molybdenite, was used for the Re–Os dating of molybdenite. The resulting age (383.2 ± 1.5 Ma; Zachariáš and Stein 2001) is in disagreement with the Ar–Ar plateau age of the sericite (339.0 ± 1.5 Ma; Zachariáš et al. 2013), common in the other Q2 samples. The higher Ti content in the molybdenite-bearing quartz (4–5 ppm Ti; Fig. 4a) may thus be considered as indirect evidence of its different origin. The presence of an older hydrothermal Mo-bearing quartz-vein system within the otherwise spatially dominating 339 Ma old gold-bearing quartz veins is possible (the oldest intrusive activity within the CBPC dates back to ~385 Ma; Košler et al. 1993). However, new, independent confirmation of the ~380 Ma Re–Os age is required (note that molybdenite is extremely rare at the Jílové deposit).

5.4.4. Quartz from the studied Bohemian gold deposits – summary

The high-temperature ("Au") deposits can be distinguished from the other Bohemian Au deposits by the elevated contents of Ti and the low contents of Sb. Other groups have a similar distribution of Ti. All of the groups exhibit only subtle variations in the Pb and Ge concentrations. Antimony-bearing Au deposits can be characterized by elevated Sb and, to some extent, also Al contents. A discernible imprint of an Sb-bearing fluid on the quartz chemistry has been observed not only at the Kasejovice and Krásná Hora deposits (the latter with mineable stibnite), but also at Roudný, where arsenopyrite contains only a minor Sb admixture (up to 4 wt. % of Sb; Zachariáš et al. 2004).

There is no clear pattern that could be used for simple discrimination between the various deposit subgroups based on the quartz trace-element contents alone. The most accurate classification of individual quartz vein types and quartz generations, prior to trace-element studies, is highly recommended. Then subtle differences in the quartz chemistry can help to interpret the quartz vein succession and fluid sources.

5.5. Comparison of Bohemian and global gold deposits

The genetic classification of the studied Au deposits has not yet been firmly established and may vary from intrusion-related gold deposits to orogenic gold deposits. Orogenic gold deposits are spatially related to the deep-crustal tectonic zones within greenschist- to amphibolite-facies terrains (e.g. Groves et al. 2003). The tectonic zones served as conduits for focused flow of deep-seated H_2O–CO_2-dominated fluids (e.g. Ridley and Diamond 2000). The intrusion-related gold deposits show spatial, temporal and genetic relationships to granitic plutons/bodies (e.g. Thompson et al. 1999; Lang and Baker 2001) and are usually formed from H_2O–CO_2-dominated fluids (e.g. Baker 2002).

When plotted, most of our data points fall in between the fields of orogenic gold and porphyry deposits (Fig. 7), as previously summarized by Rusk (2012). There is a moderate separation of the high-temperature "Au" deposits from the other Bohemian gold deposits. The bulk of the data from the moderate-to-low temperature "Au", "Au–Ag" and "Sb–Au" deposits falls within the field of orogenic gold deposits.

The two high-temperature "Au" deposits (Mokrsko, Petráčkova hora) exhibit spatial, temporal and, in some details, also a genetic affiliation to the evolution of granitic magmas/rocks of the CBPC. Both deposits were classified controversially in the past. The Petráčkova hora deposit, ini-

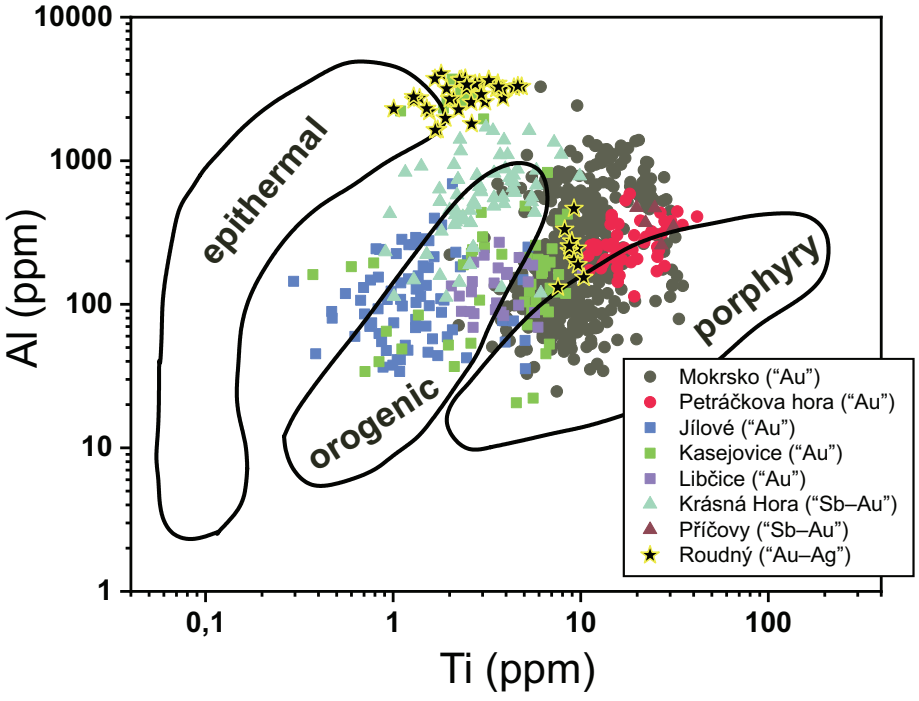

Fig. 7 The titanium versus aluminum concentrations in the hydrothermal quartz of the studied Bohemian Au deposits compared to fields for the ore-deposit types after Rusk (2012, fig. 14.10).

tially identified as a porphyry-gold type (Zachariáš et al. 2001), was later redefined as an intrusion-related gold type (Zachariáš et al. 2013). The Mokrsko deposit was classified as an intermediate member between the intrusion-related and orogenic gold types (Zachariáš et al. 2014) or as an intrusion-related gold deposit type (Zachariáš et al. 2013). The "controversial" classification of the two deposits fits in perfectly with their position between the fields of orogenic gold and porphyry deposits as defined by Rusk (2012). Note the higher content of Al (assuming fixed Ti) or the lower Ti content (assuming fixed Al) in the quartz of the Mokrsko and Petráčkova hora deposits, compared to the porphyry group of Rusk (2012). We believe this is a result of the lower formation temperature, higher pressure and different pH during the formation (in contrast to classical Cu and Cu–Au porphyry deposits).

The data of the "Au–Ag" Roudný deposit plot as two well-separated groups (Fig. 7). This dichotomy is in full accordance with the inferred occurrence of two compositionally distinct fluids and several generations of quartz veins (Zachariáš et al. 2009; Zachariáš and Hübst 2012). The early hydrothermal stages were formed from metamorphic low-salinity aqueous–carbonic fluids (H_2O–CO_2–CH_4–NaCl–$CaCl_2$), analogous to those identified at most "Au" deposits (e.g., Mokrsko, Jílové or Kasejovice). The formation of the "invisible gold" hosted by the As-rich pyrite (Zachariáš et al. 2004; gold-1 after Zachariáš et al. 2009) can also be linked to these fluids. However, the bulk of the vein quartz precipitated from medium-to-low temperature, medium-salinity aqueous fluids (H_2O–NaCl–$CaCl_2$; main-to-late hydrothermal stages), concurrently with the macroscopic gold aggregates (gold-2 after Zachariáš et al. 2009; newly introduced gold).

6. Conclusions

Analyses of hydrothermal quartz from eight Variscan vein-type Au, Au–Ag and Sb–Au deposits in the central part of the Bohemian Massif were carried out by LA-ICP-MS. In addition to the ore-bearing veins, the pre- and post-ore barren quartz veins have also been studied. Most analyzed elements approach log-normal distributions. Significant variations have been found in the contents of Al and Sb (up to two to three orders of magnitude).

The content of Ti in the ore-bearing quartz exhibits a bimodal distribution. The "Au" deposits with an assumed high-temperature origin yield a higher median value of Ti (9.7 ppm) than the other "Au" deposits (2.7 ppm) in the studied region. The difference in the Ti distribution in quartz veins between the higher and medium-to-low temperature "Au" deposits has been demonstrated to be statistically significant. The threshold value of 8 ppm Ti allows discrimination between them.

If hydrothermal quartz is associated with the Sb-bearing phase, which represents the main ore-phase (e.g. stibnite at Sb–Au deposits), then the bulk of this quartz contains over 100 ppm Sb. If the Sb-bearing phases are minor on a deposit scale, then the associated quartz is still Sb-enriched, compared to quartz from deposits with no such phases.

The concentrations of Ti and Al in the hydrothermal quartz from the ore-bearing veins of the studied Bohemian gold deposits mostly plot within and in between the fields of orogenic gold and porphyry deposits. Two Bohemian deposits (Petráčkova hora and Mokrsko) with an affiliation to the intrusion-related gold deposit type differ from the other studied deposits in their higher Ti contents and significantly overlap with the field of porphyry deposits.

Acknowledgements. This research was supported by the Grant Agency of Charles University (project GAUK 392715). Part of the equipment used for this study was purchased with funds from the Operational Programme Prague Competitiveness (Project CZ.2.16/3.1.00/21516). Also, we thank Madelaine Štulíková for editing the English language manuscript and Josef Ježek for consultations on the statistical methods. We would also like to express appreciation for the highly constructive comments by Lukáš Ackerman and one anonymous reviewer, and further to Brian Rusk and two anonymous reviewers of an early version of this manuscript. Our thanks also go to Martin Svojtka and Vojtěch Janoušek for editorial handling.

Electronic supplementary material. Supplementary table of analytical data, detection limits and basic description statistics is available online at the Journal web site (*http://dx.doi.org/10.3190/jgeosci.279*).

References

Ackerman L, Haluzová E, Creaser RA, Pašava J, Veselovský F, Breiter K, Erban V, Drábek M (2017) Temporal evolution of mineralization events in the Bohemian Massif inferred from the Re–Os geochronology of molybdenite. Miner Depos 52: 651–662

Ackerman L, Žák K, Haluzová E, Creaser RA, Svojtka M, Pašava J, Veselovský F (in print) Chronology of the Kašperské Hory orogenic gold deposit, Bohemian Massif, Czech Republic. Miner Depos, DOI 10.1007/s00126-018-0822-4

Anderson EB (1987) Isotopic–geochronological investigation of the uranium deposits of Czechoslovakia. Unpub-

lished Czechoslovak Uranium Industry Report 1862-87, pp 1–32 (in Russian)

Arapov JA, Bojcov VJ, Česnokov NI, Djakonov AV, Halbrštát J, Jakovjenko AM, Kolek M, Komínek J, Kozyrev VN, Kremčukov GA, Lažanský M, Milovanov IA, Nový V, Šorf F (1984) Czechoslovak Uranium Deposits. Czechoslovak Uranium Industry, Příbram, pp 1–368 (in Czech)

Baker T (2002) Emplacement depth and carbon dioxide-rich fluid inclusions in intrusion-related gold deposits. Econ Geol 97: 1111–1117

Bernard JH (1981) Mineralogy of Czechoslovakia. Academia, Prague, pp 1–648 (in Czech)

Bernard JH, Krs M, Morávek P, Polanský J (1983) Endogenous mineralization in the Bohemian Massif in relation to global tectonics concepts: confrontation of the geophysics and metallogeny. Sbor Geol věd, Už geofyz 18: 11–51

Boiron MC, Barakat A, Cathelineau M, Banks DA, Ďurišová J, Morávek P (2001) Geometry and P–V–T–X conditions of microfissural ore fluid migration: the Mokrsko gold deposit (Bohemia). Chem Geol 173: 207–225

Breiter K, Müller A (2009) Evolution of rare-metal granitic magmas documented by quartz chemistry. Eur J Mineral 21: 335–346

Breiter K, Svojtka M, Ackerman L, Švecová K (2012) Trace element composition of quartz from the Variscan Altenberg–Teplice caldera (Krušné hory/Erzgebirge Mts, Czech Republic/Germany): insights into the volcano–plutonic complex evolution. Chem Geol 326: 36–50

Breiter K, Ackerman L, Svojtka M, Müller A (2013) Behavior of trace elements in quartz from plutons of different geochemical signature: a case study from the Bohemian Massif, Czech Republic. Lithos 175–176: 54–67

Breiter K, Ackerman L, Ďurišová J, Svojtka M, Novák M (2014) Trace element composition of quartz from different types of pegmatites: a case study from the Moldanubian Zone of the Bohemian Massif (Czech Republic). Mineral Mag 78: 703–722

Breiter K, Ďurišová J, Dosbaba M (2017) Quartz chemistry – a step to understanding magmatic–hydrothermal processes in ore-bearing granites: Cínovec/Zinnwald Sn–W–Li deposit, Central Europe. Ore Geol Rev 90: 25–35

Campbell AJ, Humayun M (1999) Trace element microanalysis in iron meteorites by laser ablation ICPMS. Anal Chem 71: 939–946

Cruz-Uribe AM, Mertz-Kraus R, Zack T, Feineman MD, Woods G, Jacob DE (2016) A new LA-ICP-MS method for Ti in quartz: implications and application to high pressure rutile–quartz veins from the Czech Erzgebirge. Geostand Geoanal Res 41: 29–40

Dallmeyer RD, Franke W, Weber K (eds) (1995) Pre-Permian Geology of Central and Eastern Europe. Springer-Verlag, Berlin, pp 1–593

Fediuk F (1992) Metaboninite in the Proterozoic Jílové Belt of Central Bohemia. Věst Ústř Úst Geol 67: 297–310

Franěk J, Schulmann K, Lexa O, Tomek Č, Edel JB (2011a) Model of syn-convergent extrusion of orogenic lower crust in the core of the Variscan belt: implications for exhumation of high-pressure rocks in large hot orogens. J Metamorph Geol 29: 53–78

Franěk J, Schulmann K, Lexa O, Ulrich S, Štípská P, Haloda J, Týcová P (2011b) Origin of felsic granulite microstructure by heterogeneous decomposition of alkali feldspar and extreme weakening of orogenic lower crust during the Variscan Orogeny. J Metamorph Geol 29: 103–130

Franke W (2000) The middle-European segment of the Variscides: tectonostratigraphic units, terrane boundaries and plate tectonic evolution. In: Franke W, Haak U, Oncken O, Tanner D (eds) Orogenic Processes: Quantification and Modelling in the Variscan belt. Geological Society, London, Special Publications 179: 35–61

Friedl G (1997) U/Pb Datierungen an Zirkonen und Monaziten aus Gesteinen vom österreichischen Anteil der Böhmischen Masse. Unpublished PhD. thesis, Universität Salzburg, pp 1–242

Garate-Olave I, Müller A, Roda-Robles E, Gil-Crespo PP, Pesquera A, (2017) Extreme fractionation in a granite–pegmatite system documented by quartz chemistry: the case study of Tres Arroyos (Central Iberian Zone, Spain). Lithos 286: 162–174

Götze J, Möckel R (2012) Quartz: Deposits, Mineralogy and Analytics. Springer, Berlin, pp 1–360

Groves DI, Goldfarb RJ, Robert F, Hart CJR (2003) Gold deposits in metamorphic belts: overview of current understanding, outstanding problems, future research, and exploration significance. Econ Geol 98: 1–29

Hajná J, Žák J, Kachlík V (2011) Structure and stratigraphy of the Teplá–Barrandian Neoproterozoic, Bohemian Massif: a new plate-tectonic reinterpretation. Gondwana Res 19: 495–508

Holub F, Machart J, Manová M (1997) The Central Bohemian Plutonic Complex: geology, chemical composition and genetic interpretation. Sbor Geol Věd, ložisk Geol Mineral 31: 27–50

Hrstka T, Dubessy J, Zachariáš J (2011) Bicarbonate-rich fluid inclusions and hydrogen diffusion in quartz from the Libčice orogenic gold deposit, Bohemian Massif. Chem Geol 281: 317–332

Huang R, Audétat A (2012) The titanium-in-quartz (TitaniQ) thermobarometer: a critical examination and re-calibration. Geochim Cosmochim Acta 84: 75–89

Jacamon F, Larsen RB (2009) Trace element evolution of quartz in the charnockitic Kleivan granite, SW-Norway:

the Ge/Ti ratio of quartz as an index of igneous differentiation. Lithos 107: 281–291

Janoušek V, Gerdes A (2003) Timing the magmatic activity within the Central Bohemian Pluton, Czech Republic: conventional U–Pb ages for the Sázava and Tábor intrusions and their geotectonic significance. J Czech Geol Soc 48: 70–71

Janoušek V, Rogers G, Bowes DR (1995) Sr–Nd isotopic constraints on the petrogenesis of the Central Bohemian Pluton, Czech Republic. Geol Rundsch 84: 520–534

Janoušek V, Braithwaite CJR, Bowes DR, Gerdes A (2004) Magma-mixing in the genesis of Hercynian calc-alkaline granitoids: an integrated petrographic and geochemical study of the Sázava intrusion, Central Bohemian Pluton, Czech Republic. Lithos 78: 67–99

Janoušek V, Wiegand BA, Žák J (2010) Dating the onset of Variscan crustal exhumation in the core of the Bohemian Massif: new U–Pb single zircon ages from the high-K calc-alkaline granodiorites of the Blatná suite, Central Bohemian Plutonic Complex. J Geol Soc, London 167: 347–360

Janoušek V, Navrátil T, Trubač J, Strnad L, Laufek F, Minařík L (2014) Distribution of elements among minerals of a single (muscovite–) biotite granite sample – an optimal approach and general implications. Geol Carpath 65: 257–272

Jochum KP, Nohl L, Herwig K, Lammel E, Stoll B, Hofmann AW (2005) GeoReM: a new geochemical database for reference materials and isotopic standards. Geostand Geoanal Res 29: 333–338

Košler J, Aftalion M, Bowes DR (1993) Mid–late Devonian plutonic activity in the Bohemian Massif: U–Pb zircon isotopic evidence from the Staré Sedlo and Mirotice gneiss complexes, Czech Republic. Neu Jb Mineral, Mh 9: 417–431

Kříbek B, Pouba Z, Skoček V, Waldhausrová J (2000) Neoproterozoic of the Teplá–Barrandian Unit as a part of the Cadomian orogenic belt: a review and correlation aspects. Bull Czech Geol Surv 75: 175–196

Landtwing MR, Pettke T (2005) Relationships between SEM-cathodoluminescence response and trace-element composition of hydrothermal vein quartz. Amer Miner 90: 122–131

Lang JR, Baker T (2001) Intrusion-related gold systems: the present level of understanding. Miner Depos 36: 477–489

Larsen RB, Polve M, Juve G (2000) Granite pegmatite quartz from Evje-Iveland: trace element chemistry and implications for the formation of high-purity quartz. NGU-Bull 436: 57–66

Linnemann U, Pereira F, Jeffries TE, Drost K, Gerdes A (2008) The Cadomian Orogeny and the opening of the Rheic Ocean: the diacrony of geotectonic processes constrained by LA-ICP-MS U–Pb zircon dating (Ossa-Morena and Saxo-Thuringian zones, Iberian and Bohemian massifs). Tectonophysics 461: 21–43

Maydagán L, Franchini M, Rusk BG, Lentz DR, McFarlane C, Impiccini A, Ríos FJ, Rey R (2015) Porphyry to epithermal transition in the Altar Cu–(Au–Mo) deposit, Argentina, studied by cathodoluminescence, LA-ICP-MS, and fluid inclusion analysis. Econ Geol 110: 889–923

Monecke T, Kempe U, Götze J (2002) Genetic significance of the trace element content in metamorphic and hydrothermal quartz: a reconnaissance study. Earth Planet Sci Lett 202: 709–724

Monnier L, Lach P, Salvi S, Melleton J, Bailly L, Béziat D, Monnier Y, Gouy S (2018) Quartz trace-element composition by LA-ICP-MS as proxy for granite differentiation, hydrothermal episodes, and related mineralization: the Beauvoir Granite (Echassières district), France. Lithos 320: 355–377

Morávek P (1971) Ore-deposits structure and mineralization of the Jílové gold-mining district. Sbor Geol Věd, ložisk Geol Mineral 13: 1–170 (in Czech with extensive English summary)

Morávek P, Janatka J, Pertoldová J, Straka E, Ďurišová J, Pudilová M (1989) Mokrsko gold deposit – the largest gold deposit in the Bohemian Massif, Czechoslovakia. In: Keays RR, Ramsay WRH, Groves DI (eds) The Geology of Gold Deposits: The Perspective in 1988. Econ Geol Monograph 6: 252–259

Morávek P, Pouba Z, Janatka J, Malec J, Novák F, Litochleb J, Váňa T, Veselý J, Vaněček M, Kalenda Z, Aichler J, Hauk J, Skácel J, Punčochář M, Mrázek I, Tásler R, Klomínský J, Duda J, Ďurišová J, Sztacho P, Pudilová M, Soukup B, Šponar P, Doškář Z, Květoň P (1992) Gold in the Bohemian Massif. Czech Geological Survey, Prague, pp 1–245 (in Czech with extensive English summary)

Müller A, Kronz A, Breiter K (2002) Trace elements and growth patterns in quartz: a fingerprint of the evolution of the subvolcanic Podlesí granite system (Krušné hory Mts., Czech Republic). Bull Czech Geol Surv 77: 135–145

Müller A, Herrington R, Armstrong R, Seltmann R, Kirwin DJ, Stenina NG, Kronz A (2010) Trace elements and cathodoluminescence of quartz in stockwork veins of Mongolian porphyry-style deposits. Miner Depos 45: 707–727

Němec M, Zachariáš J (2018) The Krásná Hora, Milešov and Příčovy Sb–Au ore deposits, Bohemian Massif: mineralogy, fluid inclusions and stable isotope constraints on the deposit formation. Miner Depos 53: 225–244

Norman MD, Griffin WL, Pearson NJ, Garcia MO, O'Reilly SY (1998) Quantitative analysis of trace element abundances in glasses and minerals: a comparison of laser ablation inductively coupled plasma mass spec-

trometry, proton microprobe and electron microprobe data. J Anal At Spectrom 13: 477–482

O'Brien PJ (2000) The fundamental Variscan problem: high-temperature metamorphism at different depths and high-pressure metamorphism at different temperatures. In: Franke W, Haak V, Oncken O, Tanner D (eds) Orogenic Processes: Quantification and Modelling in the Variscan Belt. Geological Society, London, Special Publications 179: 369–386

O'Brien PJ, Rötzler J (2003) High-pressure granulites: formation, recovery of peak conditions and implications for tectonics. J Metamorph Geol 21: 3–20

Pták J (1962) The question of post-Variscan mineralization in the Bohemian Massif: example of vein indications in the Permo–Carboniferous relic near the Český Brod. Věst Ústř Úst Geol 37: 444–454 (in Czech with German summary)

Ridley JR, Diamond LW (2000) Fluid chemistry of orogenic lode gold deposits and implications for genetic models. In: Hagemann SG, Brown PE (eds) Gold in 2000. Reviews in Economic Geology 13: 141–162

Rusk BG (2012) Cathodoluminescent textures and trace elements in hydrothermal quartz. In: Götze J, Möckel R (eds) Quartz: Deposits, Mineralogy and Analytics. Springer, Berlin, pp 307–329

Rusk BG, Lowers HA, Reed MH (2008) Trace elements in hydrothermal quartz: relationships to cathodoluminescent textures and insights into vein formation. Geology 36: 547–550

Rusk BG, Koenig A, Lowers H (2011) Visualizing trace element distribution in quartz using cathodoluminescence, electron microprobe, and laser ablation-inductively coupled plasma-mass spectrometry. Amer Miner 96: 703–708

Schulmann K, Kröner A, Hegner E, Wendt I, Konopásek J, Lexa O, Štípská P (2005) Chronological constraints on the pre-orogenic history, burial and exhumation of deep-seated rocks along the eastern margin of the Variscan Orogen, Bohemian Massif, Czech Republic. Amer J Sci 305: 407–448

Schulmann K, Lexa O, Štípská P, Racek M, Tajčmanová L, Konopásek J, Edel JB, Peschler A, Lehmann J (2008) Vertical extrusion and horizontal channel flow of orogenic lower crust: key exhumation mechanisms in large hot orogens? J Metamorph Geol 26: 273–297

Schulmann K, Konopásek J, Janoušek V, Lexa O, Lardeaux JM, Edel JB, Štípská P, Ulrych S (2009) An Andean type Palaeozoic convergence in the Bohemian Massif. C R Geosci 341: 266–286

Strnad L, Mihaljevič M, Šebek O (2005) Laser ablation and solution ICP-MS determination of REE in USGS BIR-1G, BHVO-2G and BCR-2G glass reference materials. Geostand Geoanal Res 29: 303–314

Škácha P, Goliáš V, Sejkora J, Plášil J, Strnad L, Škoda R, Ježek J (2009) Hydrothermal uranium–base metal mineralization of the Jánská vein, Březové Hory, Příbram, Czech Republic: lead isotopes and chemical dating of uraninite. J Geosci 54: 1–13

Thomas JB, Watson EB, Spear FS, Shemella PT, Nayak SK, Lanzirotti A (2010) TitaniQ under pressure: the effect of pressure and temperature on the solubility of Ti in quartz. Contrib Mineral Petrol 160: 743–759

Thomas JB, Watson EB, Spear FS, Wark DA (2015) TitaniQ recrystallized: experimental confirmation of the original Ti-in-quartz calibrations. Contrib Mineral Petrol 169: 27

Thompson J FH, Sillitoe RH, Baker T, Lang JR, Mortensen JK (1999) Intrusion related gold deposits associated with tungsten–tin provinces. Miner Depos 34: 323–334

Tiepolo M, Bottazzi P, Palenzona M, Vannucci R (2003) A laser probe coupled with ICP–Double-focusing sector-field mass spectrometer for in situ analysis of geological samples and U–Pb dating of zircon. Canad Mineral 41: 259–272

Waldhausrová J (1984) Proterozoic volcanites and intrusive rocks of the Jílové Zone in Central Bohemia. Krystalinikum 17: 77–97

Wark DA, Watson EB (2006) The TitaniQ: a titanium-in-quartz geothermometer. Contrib Mineral Petrol 152: 743–754

Weil JA (1984) A review of electron spin spectroscopy and its application to the study of paramagnetic defects in crystalline quartz. Phys Chem Miner 10: 149–165

Wertich V, Leichmann J, Dosbaba M, Götze J (2018) Multi-stage evolution of gold-bearing hydrothermal quartz veins at the Mokrsko gold deposit (Czech Republic) based on cathodoluminescence, spectroscopic, and trace elements analyses. Minerals 8: 335, DOI 10.3390/min8080335

Zachariáš J (2016) Structural evolution of the Mokrsko–West, Mokrsko–East and Čelina gold deposits, Bohemian Massif, Czech Republic: role of fluid overpressure. Ore Geol Rev 74: 170–195

Zachariáš J, Hübst Z (2012) Structural evolution of the Roudný gold deposit, Bohemian Massif: a combination of paleostress analysis and review of historical documents. J Geosci 57: 87–103

Zachariáš J, Němec M (2017) Gold to aurostibite transformation and formation of Au–Ag–Sb phases: the Krásná Hora deposit, Czech Republic. Mineral Mag 81: 987–999

Zachariáš J, Pudilová M (2002) Fluid inclusion and stable isotope study of the Kasejovice gold district, central Bohemia. Bull Czech Geol Surv 77: 157–165

Zachariáš J, Stein H (2001) Re–Os ages of Variscan hydrothermal gold mineralizations, Central Bohemian metallogenetic zone. In: Piestrzyński A et al. (eds) Mineral Deposits at the Beginning of the 21st Century. Swets & Zeitlinger Publishers Lisse, pp 851–854

Zachariáš J, Wilkinson JJ (2007) Exlam 2000: Excel VBA application for processing of transient signals from laser ablation (LA-ICP-MS) of fluid inclusions and solid phases. In: Diamond LW, Pettke T, Spandler C (eds) European Current Research on Fluid Inclusions (ECROFI–XIX). University of Bern, Switzerland, 17–20 July, 2007, pp 194

Zachariáš J, Pudilová M, Žák K, Morávek P, Litochleb J, Váňa T, Pertold Z (1997) P–T conditions, fluid inclusions and O, C, S isotope characteristics of gold-bearing mineralizations within the Central Bohemian Metallogenic Zone. Acta Univ Carol, Geol 41: 167–178

Zachariáš J, Pertold Z, Pudilová M, Žák K, Pertoldová J, Stein H, Markey R (2001) Geology and genesis of Variscan porphyry-style gold mineralization, Petráčkova hora deposit, Bohemian Massif, Czech Republic. Miner Depos 36: 517–541

Zachariáš J, Frýda J, Paterová B, Mihaljevič M (2004) Arsenopyrite and As-bearing pyrite from the Roudný deposit, Bohemian Massif. Mineral Mag 68: 31–46

Zachariáš J, Paterová B, Pudilová M (2009) Mineralogy, fluid inclusion, and stable isotope constraints on the genesis of the Roudný Au–Ag deposit, Bohemian Massif. Econ Geol 104: 53–72

Zachariáš J, Žák K, Pudilová M, Snee LW (2013) Multiple fluid sources/pathways and severe thermal gradients during formation of the Jílové orogenic gold deposit, Bohemian Massif, Czech Republic. Ore Geol Rev 54: 81–109

Zachariáš J, Morávek P, Gadas P, Pertoldová J (2014) The Mokrsko–West gold deposit, Bohemian Massif, Czech Republic: mineralogy, deposit setting and classification. Ore Geol Rev 58: 238–263

Žák K, Vlašímský P, Snee LW (1998) $^{40}Ar/^{39}Ar$ cooling ages of selected rocks of the Příbram ore region and the question of timing of sulfidic hydrothermal mineralization. Zpr geol Výzk v Roce 1997, pp 172–173 (in Czech)